

Observations and Parameters of RT Andromedae, an Eclipsing Binary Star System

Evan Muskopf

*This work was submitted as part of a course requirement for completion of the BS degree in the Physics Program at RIT and, in its current form, does not appear in any publication external to RIT.**

(Dated: May 5, 2021)

The brightness of eclipsing binary star systems can be used to determine physical parameters of these stars. In this Capstone, we will look at a specific eclipsing binary star system, RT Andromedae. Observations of this binary star system were taken at the RIT Observatory and then analyzed. We used AstroImageJ to reduce optical data, and we wrote Python code to create light curves from the data. Using the data from our observations, we calculated the mass ratio, radius, separation distance, and temperature ratio of the two stars. We used a string length method to establish the period. To estimate the uncertainty of the period we used the jackknife resampling technique. Times of minima were determined by inspection of the light curves. These times of minima were used in combination with historical data to create an Observed Minus Calculated (O-C) diagram. This O-C diagram shows that the period of the system is currently decreasing.

Introduction

During the late 1600's, astronomers in Italy observed stars whose luminosity periodically significantly diminished. During the late 1700's, astronomer William Herschel observed, and then catalogued, approximately 700 pairs of stars. Based on the changes in luminosity, Herschel determined that the stars revolved around each other, and that the change in brightness was due to one star eclipsing the other¹. Herschel coined the term "binary" to describe these types of stars. In 1802, Herschel asserted his theory that gravity existed outside of Earth and he published his theory that these binary star systems were actually orbiting under mutual gravitational attraction.

A significant portion of stars in the skies are actually binary star systems. An eclipsing binary system is a star system with two or more stars whose orbit makes them periodically occlude each other when observed from Earth. In Figure 1, we see a hypothetical eclipsing binary system, with the smaller, blue star being brighter and the bigger, orange star being dimmer.

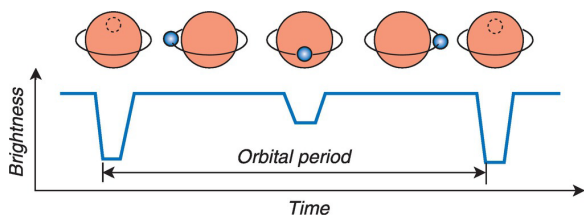


FIG. 1: Hypothetical light curve of eclipsing binary star system²

Over time, we can see that the level of luminosity increases and decreases as the stars cover and uncover each other. It is important to note that while luminosity is consistent at both maxima, when both stars are completely visible, the luminosity varies between the two minima depending on which star is being occluded. We can use the changes in the observed luminosity of the

eclipsing star system to determine characteristics of these stars.

Our target star is RT Andromedae. RT Andromedae was one of six potential eclipsing variable star systems. Selection of potential target stars was done by determining what portions of the sky would be observable during the times of night and months that we were able to observe, September-October, from 9PM to 1AM. Of the stars meeting this criterion, we then compared this information with the VizieR database to determine which stars would be bright enough to observe as well as have a period that is conducive to observation³. The results of this comparison and select parameters are listed in Table I.

Simbad Name	Maximum Magnitude	Variable Type	Period [days]	Right Ascension	Declination
V* V0523 And	11.90	EA	0.52854	01:05:37.98	+36:49:05.9
V* RT And	8.97	EA/RS	0.62892	23:11:10.10	+53:01:33.0
V* QR And	12.16	EA+NL	0.66045	00:19:49.93	+21:56:52.1
V* V0404 And	10.30	EA/RS	0.67603	01:01:24.37	+41:15:00.7
V* V0629 And	11.20	EA	0.74260	23:16:52.98	+44:29:18.3
V* V0512 And	11.80	EA	0.74532	00:52:17.30	+35:16:04.2

TABLE I: Stars observable during Capstone I that fit within the desired constraints

To choose our final target star, we used SIMBAD to find reference stars that would be usable with each of the potential targets⁴. RT Andromedae was chosen because there were several reference stars nearby with appropriate brightness, not too bright and not too dim. These nearby stars were used as reference points to calibrate

the brightness of RT Andromedae. Reference stars are needed because we can't just measure the brightness of celestial bodies because clouds and other factors change apparent brightness. When calculating the brightness of stars, we look at the difference in brightness between the reference stars and our target⁵.

RT Andromedae is located in the constellation of Andromeda. It has been the target of other scientists research in the past who have collected both light curves and spectroscopy including Pribulla et al. in 2000⁶, and Kjurkchieva, Marchev, and Ogloza, in 2001⁷. RT Andromedae is approximately 98.7 parsecs away from Earth⁴. It has a period of 0.6289216 days⁸. One star in this two star variable binary system is a K-type main-sequence star that is slightly smaller in mass than the Sun, and the other larger star is a G-type main-sequence star that is slightly larger in mass than the Sun⁶.

Observations and Data

Observations were made at the RIT Observatory over the course of the fall semester. A total of 6,890 images were taken using 4 filters; B, V, R, and I band filters. Table II lists the observation dates and the number of images taken each night in each filter.

Observation Date	B-band	V-band	R-band	I-band	Nightly Total	Weather Std. Dev.
sep04 2020	0	0	477	0	477	1433
sep14 2020	0	0	317	0	317	1144
sep20 2020	0	0	495	0	495	2533
oct16 2020	459	0	0	0	459	30566
nov03 2020	698	0	0	0	698	10231
nov06 2020	565	0	564	0	1129	10072
nov07 2020	475	0	474	0	949	7156
nov08 2020	0	437	0	436	873	3346
nov09 2020	0	385	0	385	770	2667
nov12 2020	0	0	620	0	620	2116
nov20 2020	103	0	0	0	103	54528
Total	2300	822	2947	821	6890	

TABLE II: Data gathered during each observing session. The column titled “Weather Std. Dev.” represents the standard deviation of counts for images taken on each night, with lower standard deviations generally indicating clearer skies, and higher standard deviations generally indicating cloudier skies.

Observations were made using the 12” Meade Telescope, and an Atik 11000 CCD camera using Bessel BVRI filters and a camera cooler. Calibration of the telescope mount is done by finding a bright star with a well known position near the target, then navigating to the target star and engaging the telescope’s tracking and beginning to take images. We used Altair for this purpose. Astronomical cameras need special cooling equipment in order to reduce the dark current generated by thermal excitations. After the camera has cooled, the camera must be

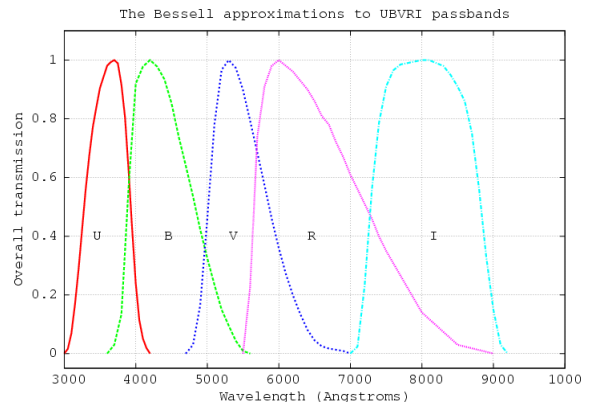


FIG. 2: Approximations of the bandpass of the UVBRI filters⁹

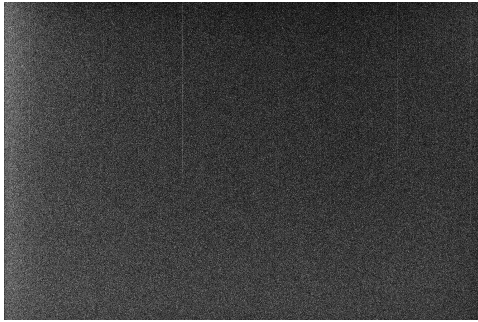
calibrated for the night. To do this, a dark image and a flatfield image must both be taken. These images are used when subtracting out dark current and correcting for defects and dust on the camera lens. After calibration, images are recorded and then analyzed.

Prior to analyzing the images, work must be done to clean up the raw data. Reducing the optical data, cleaning it up, is a multistep process; 1) obtain master dark and master flatfield frames, 2) subtract master dark frames from the raw data, and 3) then divide the resulting data by the master flatfield frames. To obtain master dark and master flatfield frames, we take multiple images and then average the data to obtain an image or frame that best represents the noise and defects that will be found in any image taken by this optical equipment. In our study, we take 20 dark frames, then take the median of these frames on a pixel-by-pixel basis and the resulting image is our master dark frame. The same process is used to create a master flatfield frame. An example of an individual flatfield frame and a dark frame from the RIT Observatory are shown in Figure 3.

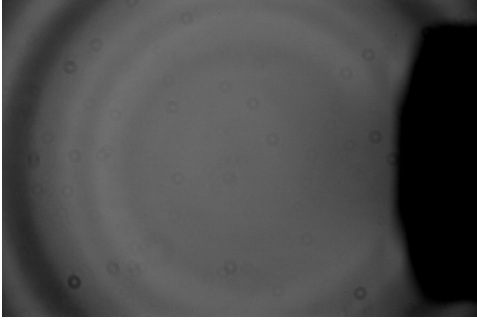
Figure 3a, is a dark frame and was taken with the lens cap on so that no light can enter the telescope. Because there is no light, the picture taken should be a picture of nothing. However, due to dark current and defects in the camera, there is something in the picture. Figure 3b is a flatfield frame and was taken with the lens cap off. It is an image of a brightly lit poster board and should be uniformly bright. However, it is not uniformly bright because of dust and vignetting by the optics.

In addition to equipment defects, dark frames are used to remove thermal noise which shows as static as can be seen in raw images. Using two images taken at the RIT Observatory, we can see the impact that defects and dark current have on raw images as shown in Figure 4. The bad column shown in the dark frame, Figure 4a is a defect in the observatory’s camera and you can see that same bad column in the raw image, Figure 4b.

At this point we have what we need to reduce the defects that will appear in any image taken. Raw data is



(a) Dark frame.



(b) Flatfield frame, dark region on the right is caused by the pick-off mirror used for tracking the sky.

FIG. 3: Calibration dark frame and flatfield frame images

cleaned up, pixel by pixel, using equation 1.

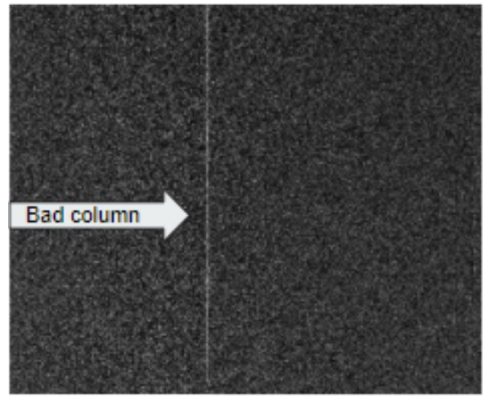
$$cleanpixel(i, j) = \frac{raw(i, j) - masterdark(i, j)}{flat(i, j)} * flatmean \quad (1)$$

The effects of noise and imaging system defects are significantly reduced in the cleaned images as shown in Figure 5. Figure 5a is an image prior to clean up, and the image in Figure 5b is the same image with optical noise reduced.

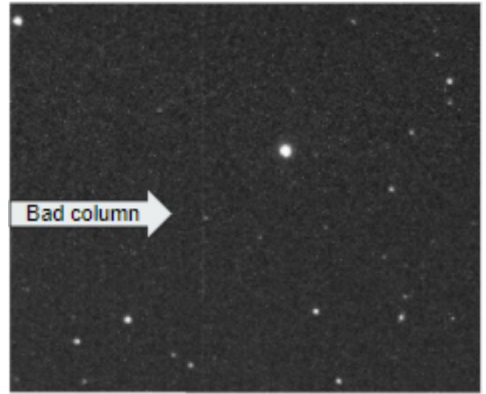
The process of cleaning the data is completed using AstroImageJ¹⁰. AstroImageJ is a public domain, astronomy-specific software package designed to calibrate and reduce noise in astronomical images. AstroImageJ produces clean images by processing the raw images with the light and dark frames as noted in Equation 1. AstroImageJ gives us the flux of my target star as well as reference stars in the clean images.

During our analysis, we noticed some very faint vertical striping on our images. To better see these vertical stripes, the contrast is increased in figure 6. While these stripes actually have very little effect on the data, it would be beneficial to remove them.

The image in Figure 6b is the product of a my preliminary attempt to remove the stripes in the data using Python. There was not enough time to determine if removing the stripes had inadvertently removed any



(a) Dark image with defect.



(b) Raw image with defect.

FIG. 4: Shown is a close up of a bad column in the dark frame and that same line shown in a raw image taken at the RIT Observatory.

meaningful data. Because of this uncertainty, the “de-striping” process was not included in our analysis process. It should be noted that this issue is not unique to our equipment at the RIT Observatory. It is possible that the issue stems from the CCD chip in the camera as this issue has been reported anecdotally from other users of the same model of CCD chip.

We can now calculate stellar brightness using this data. AstroImageJ gives us flux measured in counts. In order to use this data we have to convert to instrumental magnitude, using Equation 2.

$$\text{instrumental mag} = 25 - 2.5 * \log_{10}(\text{counts} - \text{sky}) \quad (2)$$

Instrumental magnitude is not calibrated. We can use the instrumental magnitude and the known magnitude of the reference stars to calibrate our measurements of the target star to magnitudes in the appropriate filter.



(a) Raw image.



(b) Clean image.

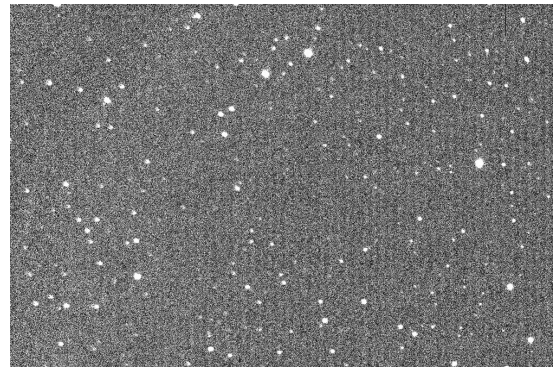
FIG. 5: Raw image, and image after clean up. The bright, noisy area on the far right of image (b) is caused by the equipment we are using, specifically, the guide camera taking some light from the main camera.

Theory

In order to classify a binary star system as eclipsing, a light curve must be obtained. A light curve is a plot of luminosity with respect to time or phase. In an eclipsing system, the light curve will show a periodic variation due to the stars eclipsing each other. An example light curve is shown in Figure 7 of star HIP 59683. A light curve of this type is often called a “folded” light curve because the phase of the system is used in the X axis instead of a set period of time such as days or hours. This star varies between about 9.19 and 9.92 magnitudes, and it has a period of 0.407528 days.

$$\text{phase} = \frac{\text{date}}{\text{period}} - \text{floor} \left(\frac{\text{date}}{\text{period}} \right) \quad (3)$$

As noted before, unless the two stars in the eclipsing system are the same temperature, the magnitude will be different during primary and secondary eclipses. This is due to one star in the pair being hotter than the other. A “primary” eclipse is when the colder star occludes the hotter star, and is shown on the light curve as the more pronounced dip. The a “secondary” eclipse is when the



(a) High contrast clean image with visible stripes.



(b) High contrast clean image with stripes removed.

FIG. 6: Images utilizing high contrast show faint vertical stripes from camera.

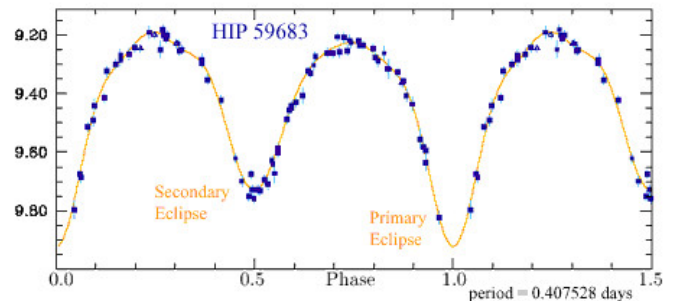


FIG. 7: Light curve of HIP 59683, with a period of 0.407528 days, taken from ESA¹¹

hotter star is occluding the colder star and is shown as the smaller dip in depth. The difference in dip depth is due to a difference in the surface brightness of the stars, which is due to different temperatures of the stars.

Light curves will vary based on eclipsing binary star parameters such as brightness of stars, temperature, size, shape of orbit, and separation. In Figure 8¹², we see representative light curves of three different types of eclipsing binary star systems, (a) EA, (b) EB and (c) EW.

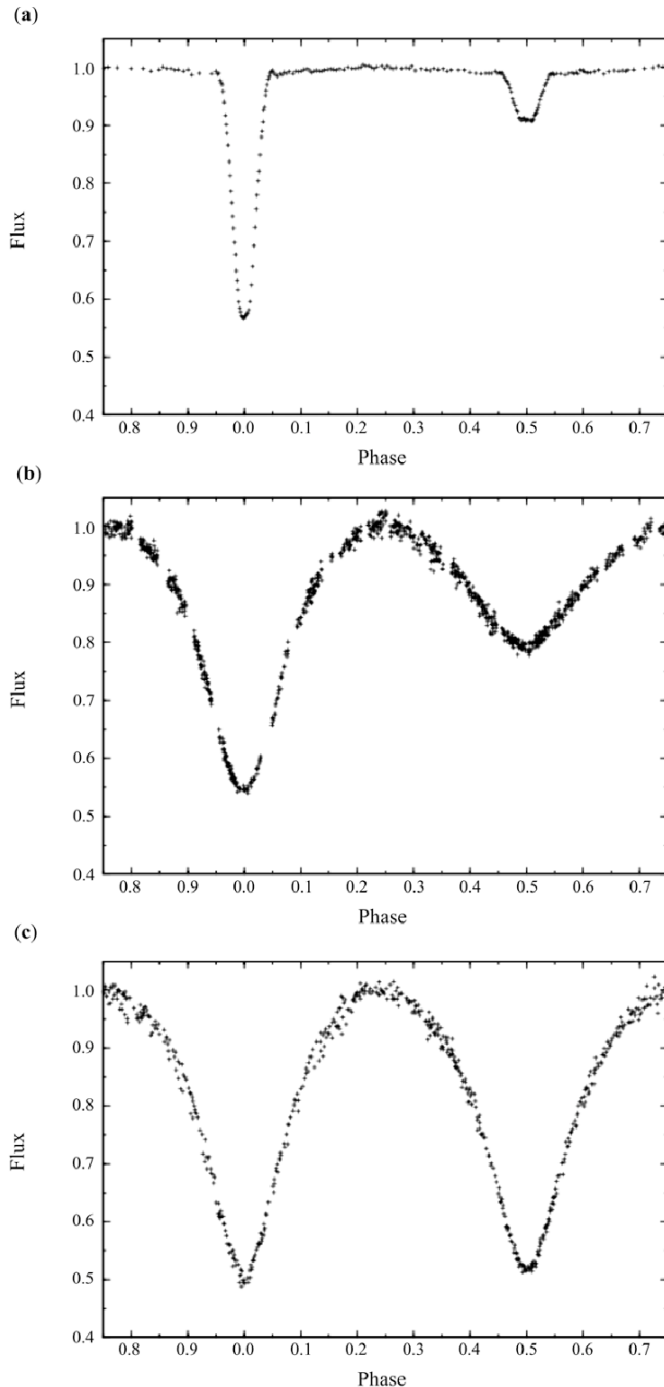


FIG. 8: We see representative light curves of three different types of eclipsing binary star systems, (a) EA, (b) EB and (c) EW. The primary and secondary eclipses for EA and EB systems show a greater difference in brightness. This is because these star systems are structured differently, EA systems are completely separate stars, EW systems are completely overlapping with a common envelope, and EB stars are in between EA and EW.¹²

Analysis

A. Light Curve Analysis

Using the images taken at the RIT Observatory, the light curve for my target star, RT Andromedae is constructed and shown in Figure 9. The light curve shows that RT Andromedae varies in R-band magnitude from 8.97 to 9.83, maximum and minimum respectively. The minimum magnitude occurs when the colder star occludes the hotter star during the primary eclipse, and the maxima occurs when neither star is occluded.

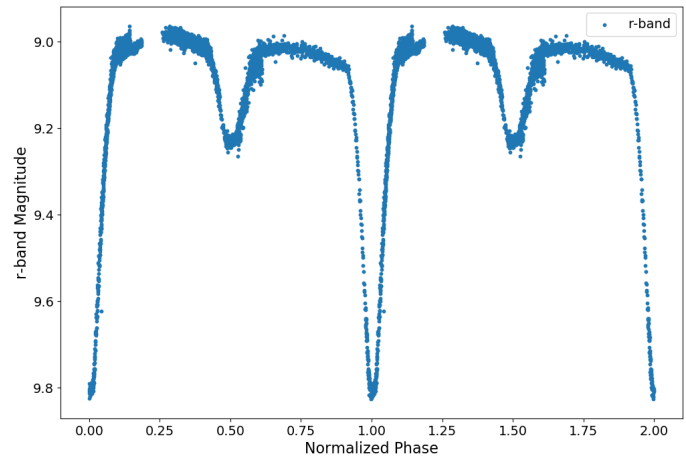


FIG. 9: R-band light curve of RT Andromedae

A light curve of our target star and the reference stars was created using data from a single night, November 7, 2020, and is shown in Figure 10. This light curve shows that the reference stars maintain a consistent magnitude, while the magnitude of RT Andromedae shows a drop during occlusion. In this light curve, the hotter star is occluding the colder star in the target system.

When the light curve of RT Andromedae is compared to the light curves in Figure 8, we see that the light curve of RT Andromedae is similar to the light curve of the EA star shown in Figure 8a. Using the comparison, we deduce that RT Andromedae is an EA type star, where the system's stars are two distinct and separate objects.

B. Potential Undiscovered Variable Star

As mentioned earlier, one of the reasons we chose to look at RT Andromedae was that there were several reference stars nearby. The blue line in the light curve in Figure 11 shows RT Andromedae returning to full brightness after an occlusion. The other lines are the reference stars. These other lines should be relatively flat, meaning consistent in magnitude. However, we found that one of our reference stars does not have consistent magnitude as can be seen by the data in orange. While this star has been observed by others in the past, it appears that this

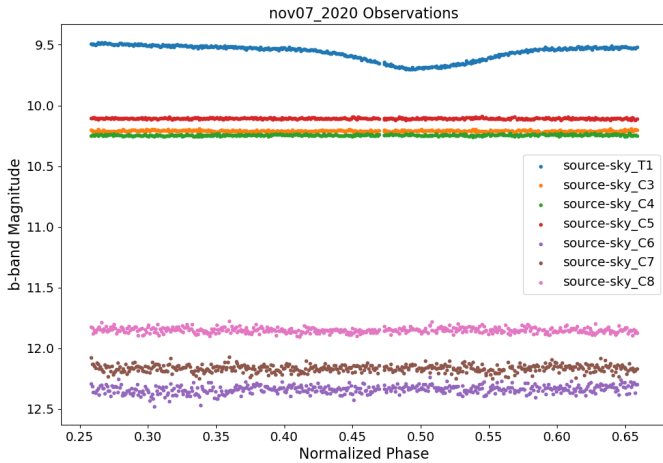


FIG. 10: Light curve of RT Andromedae in blue and reference stars in other colors

star has not been recognized as a variable star. There is a possibility that this is a previously undiscovered variable star system. We were not able to get enough data on this star before it became unobservable from our observatory, because of this we were unable to determine the period or anything else about the star.

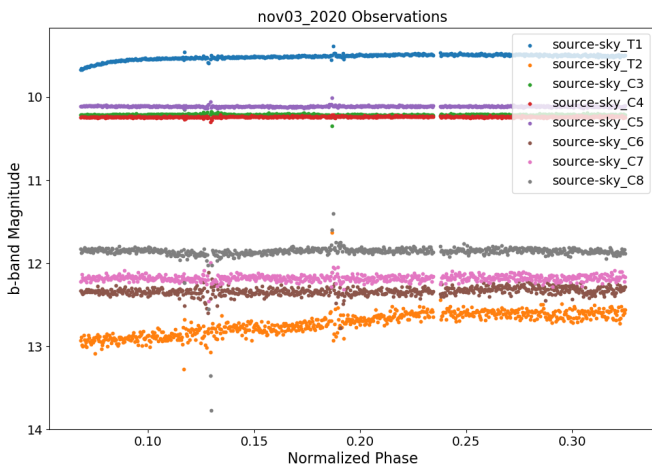


FIG. 11: Night of observations that shows strange dip in magnitude of one reference star.

C. Stellar Temperature Ratio

Different filters were used during the course of observations to obtain information that was used to determine parameters of the target star system. Figure 12 shows magnitudes recorded when different filters were placed in front of the camera. Each filter allows a specific band of wavelengths to pass through the filters.

The graph shown in Figure 13 is a graph of normalized intensity for the images obtained using the V Band fil-

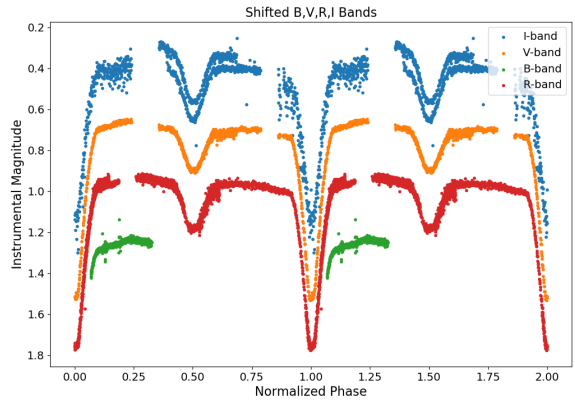


FIG. 12: The figure shows the lightcurve data taken through the B,V,R,I filters and shifted for readability

ter. We can see the different depths of the primary and secondary eclipses. We can use these depths in Equation 4 to calculate the ratio of the temperatures between the two stars in the binary system.

$$\text{temperature ratio} = \left(\frac{\text{primary depth}}{\text{secondary depth}} \right)^{\frac{1}{4}} \quad (4)$$

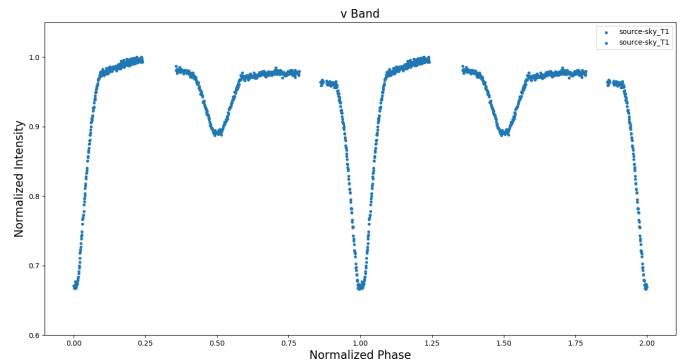


FIG. 13: V-band graph of normalized intensity

The results of the analysis in all four bands we took data in are shown in Table III. The results of this preliminary analysis are not within uncertainties of the results obtained by other researchers¹³¹⁴. Much of the discrepancy can be explained by the simplistic assumptions that we used when calculating temperature. In this paper we assumed the stars were perfect blackbodies and that they were perfect spheres.

D. Orbital Period

Determining the period of binary stars can be done by either direct observation or by calculation. The period

Filter Used	Depth of Primary Eclipse	Depth of Secondary Eclipse	Temperature Ratio
B-band	27%	10%	1.29
V-band	31%	8%	1.38
R-band	32%	7%	1.47
I-band	30%	9%	1.34

TABLE III: Calculated eclipse depths and approximate temperature ratios. These compare well but do not exactly equal values from other papers, like from Pribulla with a value of 1.27⁶

of some systems can be determined by inspection if the period is short enough to be observed fully in one observing run. However, most stars do not have a short enough period for this method to be used. By utilizing many observations of incomplete periods, it is possible to fit these observations together until a complete period is formed. This can be done manually by guessing or by using a computer to do the guessing for you. The challenge becomes how to tell the computer that it has guessed the correct period? To do this, astronomers use the string length method.¹⁵ Since the period of RT Andromedae is longer than one night, we used the string length method to determine the period of our system.

The string length method is used to establish the period of a variable star from a relatively small number of randomly spaced observations over a long span of time.¹⁵ This method assumes that using the correct period results in the smallest sum of the lengths of line segments. When calculating string length, a line segment is the line connecting individual consecutive data points. Based on this assumption, one of the ways to find the period is to keep guessing periods until you find the smallest sum of lengths. We use a computer to do this guessing for us. A correctly determined period will show multiple observing runs as one connected cycle and will place all maxima and minima overlapping correctly in phase space.

In Figure 14, four different observing runs have been plotted. Because the period is wrong, the observing runs are offset in phase.

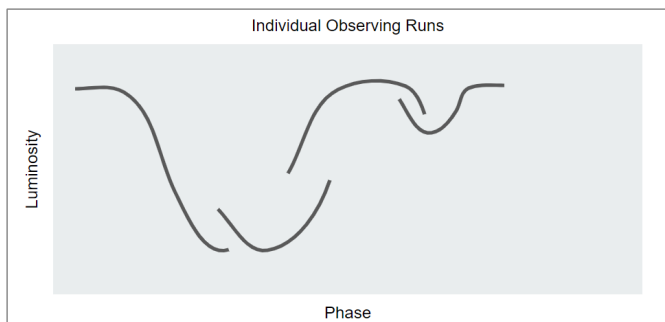


FIG. 14: Four separate observing runs of a binary system

Figure 15 is a visualization of an intermediate step

in the string length method. In this graph, the individual data points are connected consecutively in phase. Because the period is not exactly correct, zig zag lines connect the different observing runs. The longer string length caused is indicative of an incorrect period.

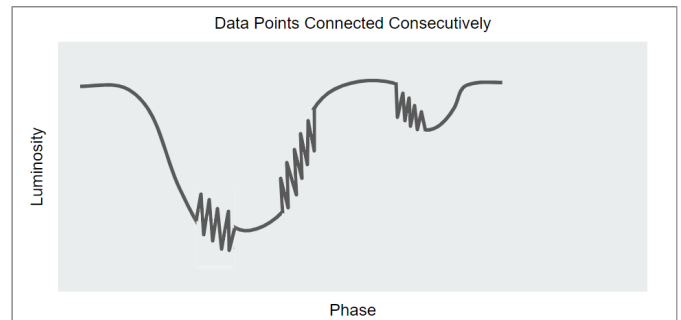


FIG. 15: Individual data points are connected consecutively

Figure 16 shows the observing runs overlapping each other as would be expected in a good period. In this case the total string length is minimized.

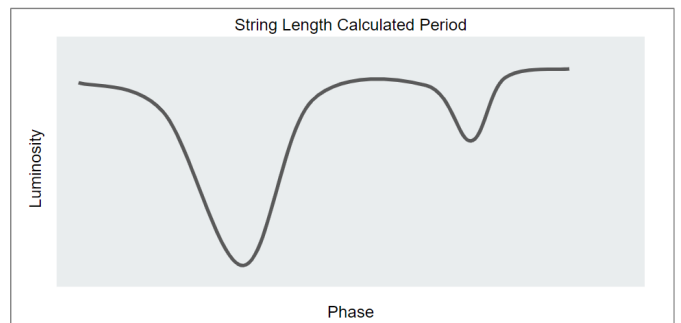


FIG. 16: Minimized string length

To obtain a measurement of the period with an uncertainty we used Jackknife Statistics with the string length method.¹⁶ Using multiple subsets of our data, multiple periods are determined. We take the average of the periods which were derived from the multiple subsets of data \pm standard deviation to determine the period with an uncertainty as noted in Equation 5

$$\text{Period} = \text{Average} \pm \text{StandardDeviation} \quad (5)$$

We observed in four bands, BVRI, over the course of three months. Four separate datasets were obtained from these observations, one dataset from each band. These datasets were used to calculate the period of the system as shown in Table IV.

Since our data was collected in a short time frame, the period of the system shouldn't vary from collection date to collection date. However, the periods of the bands are not consistent. The B and R periods agree with each

Filter Used	Period [days]	Uncertainty
B-band period	0.628913	0.000008
V-band period	0.629246	0.000055
R-band period	0.628904	0.000003
I-band period	0.630495	0.000228

TABLE IV: Periods determined using BVRI band data

other within uncertainties. The remaining bands, V and I, do not agree within uncertainties. This may be because of a limited data set.

E. Individual Star Radius

We calculated the radius of each individual star in the system utilizing Equation 6 and Equation 7. The distance covered by the stars during the eclipse is equal to the sum of both of their diameters, as well as the sum of their velocities multiplied by the duration of the eclipse. This is shown in Equation 6. While Equation 6 gives us information about the sum of the diameters, a relationship also exists for the difference in diameters as shown in Equation 7. In Equation 7, the duration of the total eclipse multiplied by the sum of the velocities is equal to the difference of diameters. These relationships are only true for circular orbits.

$$2R_A + 2R_B = (t_4 - t_1) * (v_A + v_B) \quad (6)$$

$$2R_A - 2R_B = (t_3 - t_2) * (v_A + v_B) \quad (7)$$

Eq. 6 & 7: t_1, t_2, t_3, t_4 as in Figure 17

Using Equations 6 and 7, we determined the radius of the star A to be 1.254 solar radii. Using Radius A, we then calculated the radius of star B to be 0.916 solar radii. These values are in line with the findings of other researchers⁶.

Star	Radius [solar radii]	Source
star A	1.254	Our observations
star A	1.221	Pribulla ⁶
star B	0.916	Our observations
star B	0.890	Pribulla ⁶

TABLE V: Radii of stars

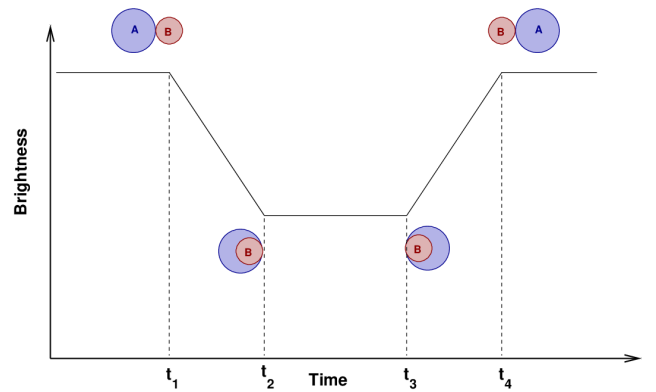


FIG. 17: t_1 is the time of first contact, it is when the stars first begin to cover each other and the eclipse has begun. t_2 is when the stars are fully covering each other and the total eclipse has begun. t_3 is when the stars begin to uncover each other and the total eclipse ends. t_4 is when the stars are no longer covering each other at all and the eclipse is over.⁹

F. Orbital Radius and Stellar Separation

To obtain the stellar separation, we must first determine the orbital radius of each star. The orbital radius is the star's distance from the center of mass. To determine the orbital radius we use Equation 8

$$v * p = 2\pi R \quad (8)$$

We use the radial velocity for each star that was previously determined by T. Pribulla⁶, $v_A=132.6$ km/s and $v_B=176.2$ km/s. Applying Equation 8, we calculate the orbital radius of Star A to be 1.648 solar radii and the orbital radius of Star B to be 2.190 solar radii. Our findings are in line with the findings of prior researchers⁶.

Source	Star	Orbital Radius [solar radii]
Our observations	star A	1.648
Our observations	star B	2.190
Our observations	stellar separation (star A + star B)	3.839
Pribulla ⁶	stellar separation (star A + star B)	3.865

TABLE VI: Orbital radius and stellar separation.

We now use the calculated orbital radii to determine the stellar separation of the system as noted in Eq. 9. This is simply the sum of the two star's orbital radius, which equals 3.839 solar radii and is consistent with prior research⁶.

$$A = R_{OA} + R_{OB} \quad (9)$$

G. Masses

To obtain the individual star masses, we needed to first calculate the total mass of the system. To do this, we use Kepler's Third Law, Equation 10, and find the total mass of the system to be 1.9188 solar masses.

$$p^2 = \frac{4\pi^2}{G(M_A + M_B)} a^3 \quad (10)$$

In a binary star system, gravity pulls each star towards the system's center of mass. Since gravity acts with the same force on both stars, the heavier star will have a lower acceleration and thus, a smaller velocity. Conversely, the less massive star will have a higher acceleration and a higher velocity. The relationship between the two star's velocities is given in Equation 11⁹.

$$\frac{v_A}{v_B} = \frac{M_B}{M_A} \quad (11)$$

This relationship can be used along with the total mass of the system to determine the individual masses of each star. We calculated the masses to be $M_A=1.095$ solar masses, $M_B=0.824$ solar masses. This falls within uncertainties of prior research⁶.

Source	Star	Mass [solar mass]
Our observations	star A	1.095
Our observations	star B	0.824
Our observations	Total Mass	1.9188
Pribulla ⁶	star A	1.083
Pribulla ⁶	star A	0.838
Pribulla ⁶	Total Mass	1.921

TABLE VII: Stellar Mass

H. Changing Period and O-C Diagrams

Our analysis of RT Andromedae's period shows that it has changed over time. We see this by inspecting an O-C diagram for this system. An O-C diagram is a graph of Observed Time of Minima minus Calculated Time of Minima. A static period would have a flat line O-C diagram. A changing period will result in a diagram that is not a flat line. Figure 18 shows three different examples. An unchanging period is represented by the blue line. In a system with an increasing period, the O-C diagram would curve upward and is represented by the green line,

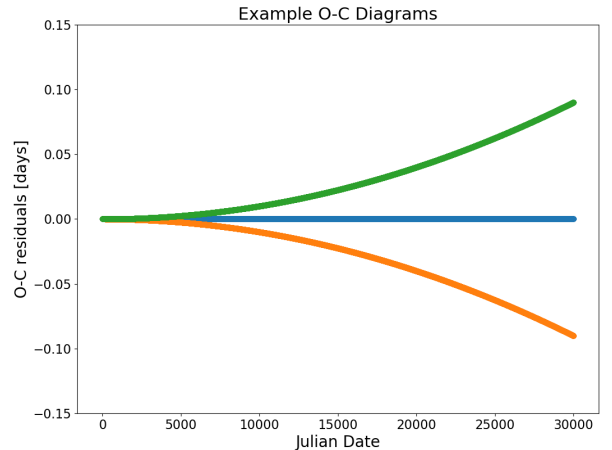


FIG. 18: Example O-C Diagrams

and in a system with a decreasing period, the O-C diagram would curve downward and is represented by the orange line.

For the stars to slow down, they would need to lose angular momentum and because angular momentum is conserved, the stars will continue to rotate with the same period unless something outside the system acts on them to change the angular momentum. While stars lose mass due to solar winds, this would not account for a change in angular velocity because mass is ejected isotropically, and there is no net change in angular velocity. A possible explanation for a decreasing period might be magnetic braking.

A portion of the particles ejected in the stellar wind are ionized. This ionized material gets caught in the magnetic field of the star. Eventually the ionized materials get far enough away from the star that the magnetic field is no longer strong enough to hold the matter, and the matter escapes. This reduces the angular momentum of the star disproportionately compared to the amount of mass lost. This is because the escaping matter has a lot of angular momentum but relatively little mass. This causes the star to slow down and the period to decrease, hence the term magnetic braking.

Another explanation for a change in observed period could be the influence of a third, unseen star. There are several reasons why a third star may not be visible. The third star may be undetectable because it is too far away to observe, because the period is too long, or because it is not in the same plane as the binary system and does not eclipse. In the case of a third star, the binary system rotates around the third star, moving closer and further away from Earth and causing the observed times of minima to shift. Because the speed of light doesn't change, when the star system is closest to Earth, the light takes the least amount of time to reach Earth and conversely, when the system is at its furthest point from Earth, the light takes the longest amount of time to reach

Earth. This causes a sinusoidal variation in the O-C diagram.

Figure 19 is an O-C diagram of RT Andromedae from the past 106 years, inclusive of historical data and our data. Our data is consistent and continues the same downward slope as recent prior researcher's data.

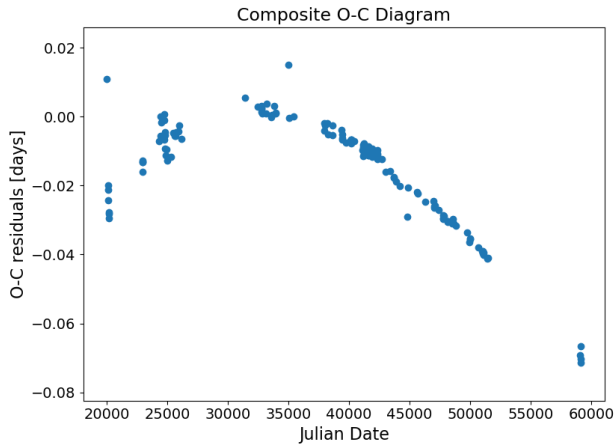


FIG. 19: Historical data taken from Pribulla⁶

Acknowledgments

This research has made use of NASA's Astrophysics Data System. This research has made use of the Stellarium planetarium.

I would like to thank the RIT School of Physics and Astronomy, both faculty and students, especially Vince Iglesias-Cardinale, for their support. Lastly, I would like to thank my mentor, Dr. Michael Richmond, for his guidance with this project, and for his support, time, and compassion over my time at RIT. Always a friendly face, Dr. Richmond will be a part of RIT that I will always remember and appreciate.

* Rochester Institute of Technology, School of Physics and Astronomy, Faculty Advisor: Dr. Richmond

¹ T. E. of Encyclopaedia Britannica, Encyclopaedia Britannica (2019), retrived online from: <https://www.britannica.com/biography/William-Herschel/Theory-of-the-evolution-of-stars>.

² C. Christian and J.-R. Roy, *Stars and Stellar Systems*, 2 ed. (Cambridge University Press, 2017), p. 75–128.

³ O. F. et. a, The VizieR database of astronomical catalogues .

⁴ M. Wenger *et al.*, *aaps* **143**, 9 (2000), arXiv:astro-ph/0002110.

⁵ J. Menke, Society for Astronomical Sciences Annual Symposium **22**, 3 (2003).

⁶ T. Pribulla *et al.*, *Astronomy and Astrophysics* **362**, 169 (2000).

⁷ D. P. Kjurkchieva, D. V. Marchev, and W. Ogloza, *Astronomy and Astrophysics* **378**, 102 (2001).

⁸ N. N. Samus', E. V. Kazarovets, O. V. Durlевич, N. N.

Kireeva, and E. N. Pastukhova, *Astronomy Reports* **61**, 80 (2017).

⁹ M. Richmond, *Eclipsing binary stars*, 2020.

¹⁰ K. A. Collins, J. F. Kielkopf, K. G. Stassun, and F. V. Hessman, *The Astronomical Journal* **153**, 77 (2017).

¹¹ Cosmos EAS: Hipparcos, Hipparcos, 1997, figure retrieved from published data, <https://www.cosmos.esa.int/web/hipparcos/home>.

¹² P. Skelton and D. Smits, *South African Journal of Science* **105**, 120 (2009).

¹³ D. Manzoori, *The Astronomical Journal* **138**, 1917 (2009).

¹⁴ Kjurkchieva, D. P., Marchev, D. V., and Ogloza, W., *A&A* **378**, 102 (2001).

¹⁵ M. M. Dworetzky, *Monthly Notices of the Royal Astronomical Society* **203**, 917 (1983).

¹⁶ B. Efron and C. Stein, *The Annals of Statistics* **9**, 586 (1981).